

## Doping-enhanced antiferromagnetism in $\text{Ca}_{1-x}\text{La}_x\text{FeAs}_2$

Shinji Kawasaki,<sup>1</sup> Tomosuke Mabuchi,<sup>1</sup> Satoki Maeda,<sup>1</sup> Tomoki Adachi,<sup>1</sup> Tasuku Mizukami,<sup>1</sup> Kazutaka Kudo,<sup>1</sup> Minoru Nohara,<sup>1</sup> and Guo-qing Zheng<sup>1,2</sup>

<sup>1</sup>*Department of Physics, and Research Center of New Functional Materials for Energy Production, Storage and Transport, Okayama University, Okayama 700-8530, Japan*

<sup>2</sup>*Institute of Physics and Beijing National Laboratory for Condensed Matter Physics, Chinese Academy of Sciences, Beijing 100190, China*

(Received 25 May 2015; revised manuscript received 29 October 2015; published 18 November 2015)

In iron pnictides, high temperature superconductivity emerges after suppressing antiferromagnetism by doping. Here, we show that antiferromagnetism in  $\text{Ca}_{1-x}\text{La}_x\text{FeAs}_2$  is robust against and even enhanced by doping. Using <sup>75</sup>As-nuclear magnetic resonance and nuclear quadrupole resonance techniques, we find that an antiferromagnetic order occurs below the Néel temperature  $T_N = 62$  K at a high doping concentration ( $x = 0.15$ ) where superconductivity sets in at the transition temperature  $T_c = 35$  K. In the superconducting state coexisting with antiferromagnetism, the nuclear-spin-lattice relaxation rate  $1/T_1$  becomes proportional to  $T$ , indicating gapless excitations. Unexpectedly,  $T_N$  is enhanced with increasing doping, rising up to  $T_N = 70$  K at  $x = 0.24$ . The obtained phase diagram of this system enriches the physics of iron-based high- $T_c$  superconductors.

DOI: [10.1103/PhysRevB.92.180508](https://doi.org/10.1103/PhysRevB.92.180508)

PACS number(s): 74.25.Dw, 74.25.nj, 74.62.Dh, 74.70.Xa

The relationship between magnetism and superconductivity is an important issue in strongly correlated electron systems. In copper oxides, carrier doping into Mott insulators suppresses the magnetic order and induces high temperature superconductivity [1]. In iron pnictides or selenides, superconductivity also emerges after the magnetic state is destroyed. For example, in  $\text{LnFeAsO}$  (1111 system,  $\text{Ln}$  = lanthanoid), the substitution of a few percent of F for O suppresses the antiferromagnetic order and induces superconductivity with the transition temperature  $T_c$  up to 55 K [2–8]. In  $\text{BaFe}_2\text{As}_2$  (122 system), the substitution of K ( $TM$  = transition metal) for Ba (Fe) introduces a hole (electron) to the system [9–12]. In either case, superconductivity appears at low doping levels of less than 10% [9–12]. In some of these compounds, magnetism can coexist microscopically with superconductivity [13,14]. Extensive studies have shown that the quantum spin fluctuations associated with the magnetic order are important for superconductivity [14–17].

However, this picture has been challenged by recent materials which suggested that the phase diagram of the iron pnictides can actually be much richer and the physics may be more diverse. With the high-pressure technique, it has been reported that one can dope carriers beyond  $x = 0.5$  [18,19]. In  $\text{LaFeAsO}_{1-x}\text{F}_x$ , although no magnetism or even magnetic fluctuations were found in the high doping region,  $T_c$  forms another dome centered at  $x \sim 0.5$  [19]. In hydride-doped  $\text{LaFeAsO}_{1-x}\text{H}_x$ ,  $T_c$  also forms another dome [18], but antiferromagnetism emerges after superconductivity disappears for  $x > 0.5$  [20,21]. The magnetism in the highly hydride-doped system is intriguing, but the origin of this antiferromagnetism and its relation to superconductivity are still unclear [21,22]. In particular, the requirement of the unconventional method (a high-pressure synthesis technique) to obtain  $\text{LaFeAsO}_{1-x}\text{H}_x$  samples prevents this interesting phenomenon from being understood. A more easily available material example is highly desired.

Recently, a new system,  $\text{Ca}_{1-x}\text{La}_x\text{FeAs}_2$  (112 type), was discovered [23–26] by the conventional synthesis technique. It crystallizes in a monoclinic structure (space group  $P2_1$ ) and consists of stacking the  $\text{Fe}_2\text{As}_2$  and the  $(\text{Ca},\text{La})_2\text{As}_2$  layers along the  $c$  axis. The pure compound  $\text{CaFeAs}_2$  cannot be

obtained, but replacing Ca with La ( $x \geq 0.15$ ) can stabilize the 112 phase. The highest  $T_c = 35$  K was found for  $x = 0.15$  [23–25]. Since one La atom introduces one electron to the  $\text{Fe}_2\text{As}_2$  layer, the doping level is high compared to the ambient-pressure-synthesized 1111 or 122 systems. With further doping beyond  $x = 0.15$ ,  $T_c$  decreases and disappears at  $x = 0.25$  [24]. The band structure calculation showed that the overall Fermi surfaces are similar to those of  $\text{LaFeAsO}_{1-x}\text{F}_x$  [23]. Interestingly, it has been confirmed that both the As-Fe-As bond angle and the lattice parameter do not change from  $x = 0.15$  to 0.25 [24,25].

In this Rapid Communication, we report a finding of a magnetic order with the Néel temperature  $T_N = 62$  K for  $\text{Ca}_{0.85}\text{La}_{0.15}\text{FeAs}_2$  with  $T_c = 35$  K by <sup>75</sup>As-nuclear magnetic resonance (NMR)/nuclear quadrupole resonance (NQR) techniques. Furthermore, we find unexpectedly that  $T_N$  increases with increasing doping, rising up to  $T_N = 70$  K for  $x = 0.24$ . Our system provides an opportunity to study the relationship between high- $T_c$  superconductivity and doping-enhanced magnetism.

Single crystals of  $\text{Ca}_{1-x}\text{La}_x\text{FeAs}_2$  ( $x = 0.15, 0.19, \text{ and } 0.24$ ) were prepared as reported elsewhere [23–25]. The La concentrations were determined by energy-dispersive x-ray spectrometry measurement. The ac susceptibility measurements using the NMR coil indicate  $T_c \sim 35$  and 34 K for  $x = 0.15$  and 0.19, respectively, but no  $T_c$  is observed for  $x = 0.24$ . The magnetization  $M$  was measured using the Quantum Design magnetic property measurement system (MPMS). In order to achieve a good signal-to-noise ratio, about 500 mg of small-sized (about 100  $\mu\text{m}$  in diameter) single crystals were collected for NMR/NQR measurements [27]. NMR/NQR spectra were taken by changing the rf frequency and recording the spin echo intensity step by step. The <sup>75</sup>As-NMR  $T_1$  was measured at the frequencies in the center transition ( $m = 1/2 \leftrightarrow -1/2$ ) peak [28].

As a typical example, Fig. 1(a) shows the <sup>75</sup>As-NMR ( $I = 3/2$ ) spectrum for  $x = 0.19$ . The nuclear spin Hamiltonian is expressed as a sum of the Zeeman and nuclear quadrupole interaction terms,  $\mathcal{H} = \mathcal{H}_z + \mathcal{H}_Q = -\gamma \hbar \mathbf{I} \cdot \mathbf{H}_0(1 + K) + (h\nu_Q/6)[3I_z^2 - I(I + 1) + \eta(I_x^2 - I_y^2)]$ , where  $\gamma = 7.292$  MHz T<sup>-1</sup>,  $h$  is Planck's constant,  $H_0$  is the

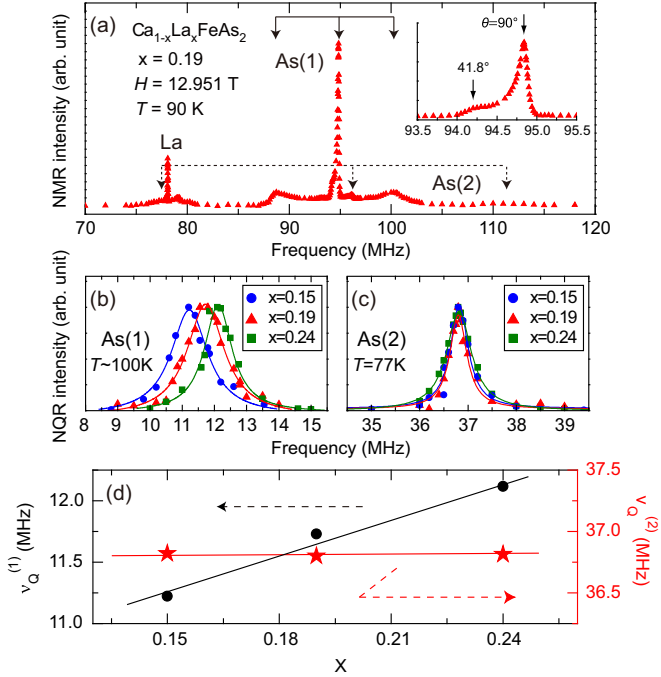


FIG. 1. (Color online) (a) NMR spectrum for  $x = 0.19$ . The inset shows the center peak for As(1). (b), (c)  $x$  dependence of the  $^{75}\text{As}$ -NQR spectra for As(1) and As(2). The solid lines are the results of Lorentzian fitting to obtain the peak position,  $\nu_Q^{\text{As}(1,2)}$ . (d)  $x$  dependence of  $\nu_Q^{\text{As}(1,2)}$ . The solid lines are a guide to the eye.

external magnetic field,  $K$  is the Knight shift, and  $I$  is the nuclear spin. NQR frequency  $\nu_Q$  and asymmetry parameter  $\eta$  are defined as  $\nu_Q = \frac{3eQV_{zz}}{2I(2I-1)\hbar}$ ,  $\eta = \frac{V_{xx}-V_{yy}}{V_{zz}}$ , with  $Q$  and  $V_{\alpha\beta}$  being the nuclear quadrupole moment and the electric field gradient (EFG) tensor at the As site, respectively [29]. As seen in the inset to Fig. 1(a), the  $^{75}\text{As}$ -NMR center transition consists of two peaks which correspond to crystallites with  $\theta = 41.8^\circ$  and  $90^\circ$ , where  $\theta$  is the angle between  $H_0$  and the principal axis of the EFG along the  $c$  axis [29]. Theoretically, the peak intensity of  $\theta = 41.8^\circ$  is higher than that of  $\theta = 90^\circ$  for a complete powder pattern [29]. However, we found the opposite, which indicates that about 50% of the tiny crystals are aligned to  $H_0$ , with  $H_0 \parallel ab$  plane. This situation allowed us to obtain  $T_1$  with the  $H_0 \parallel ab$  plane with great accuracy [28]. As shown by the solid [As(1) site] and dotted [As(2) site] arrows, we obtained two sets of  $^{75}\text{As}$ -NMR spectra, since  $\text{Ca}_{1-x}\text{La}_x\text{FeAs}_2$  has two inequivalent As sites, one in the  $\text{Fe}_2\text{As}_2$  layer and the other in the  $(\text{Ca},\text{La})_2\text{As}_2$  layer. Each set has three transitions from  $I_z = (2m+1)/2$  to  $(2m-1)/2$ , where  $m = -1, 0, 1$ . From Fig. 1(a), we estimated  $\nu_Q^{\text{As}(1)} \sim 11.5$  MHz,  $\nu_Q^{\text{As}(2)} \sim 35$  MHz, and  $\eta \sim 0$  for both sites.

Figures 1(b) and 1(c) show the NQR spectra. As summarized in Fig. 1(d),  $\nu_Q^{\text{As}(1)}$  increases with increasing doping, but  $\nu_Q^{\text{As}(2)}$  remains about the same. Since the lattice parameters do not change with doping [24], the origin of the doping dependence of  $\nu_Q$  should be the EFG generated by the doped electrons in the  $\text{Fe}_2\text{As}_2$  layer. Hence, we conclude that As(1) originates from the  $\text{Fe}_2\text{As}_2$  layer and As(2) from the  $(\text{Ca},\text{La})_2\text{As}_2$  layer. The doping dependence of  $\nu_Q^{\text{As}(1)}$  is in good agreement with that reported in  $\text{LaFeAsO}_{1-x}\text{F}_x$  [16].

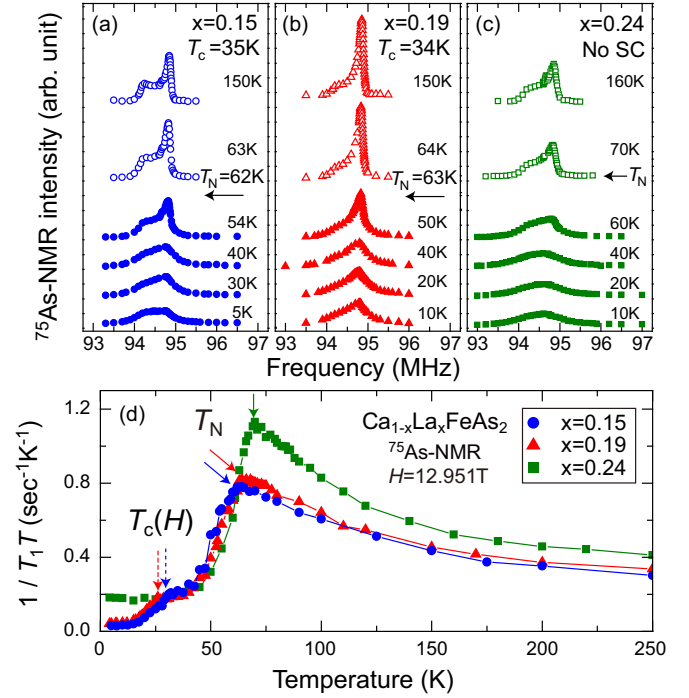


FIG. 2. (Color online) Temperature dependence of the  $^{75}\text{As}$ -NMR center peak for As(1) for (a)  $x = 0.15$ , (b)  $0.19$ , and (c)  $0.24$ , respectively. (d) Temperature dependence of  $1/T_1T$ . The solid and dotted arrows indicate  $T_N$  and  $T_c(H)$ .

To investigate the evolution of the normal-state electronic property, we measured the temperature dependence of the  $^{75}\text{As}$ -NMR center peak and  $T_1$  for As(1). As seen in Fig. 2, the  $^{75}\text{As}$ -NMR spectra unexpectedly became broad at low temperatures for all doping levels. Concomitantly,  $1/T_1T$  divided by temperature ( $1/T_1T$ ) showed a peak at  $T = 62, 63,$  and  $70$  K for  $x = 0.15, 0.19,$  and  $0.24$ , respectively. This is consistent with the critical slowing down behavior across  $T_N$  as observed in  $\text{BaFe}_2\text{As}_2$  [30] and  $\text{LaFeAsO}_{0.97}\text{F}_{0.03}$  [16], suggesting that the origin of the broadening of the NMR spectra is due to the appearance of the internal magnetic field  $H_{\text{int}}$  at the As site.

In order to further confirm the origin of the spectrum broadening, we measured the evolution of the NQR spectrum and compared it with NMR result. Figure 3(a) shows the  $^{75}\text{As}$ -NQR spectrum obtained at  $T = 70$  and  $4.2$  K for  $x = 0.24$ . Figure 3(b) shows the  $^{75}\text{As}$ -NMR spectrum at  $T = 10$  K for  $x = 0.24$  chosen from Fig. 2(c). As was observed in the NMR, the  $^{75}\text{As}$ -NQR spectrum also became broad at low temperatures. Figure 3(c) shows the temperature dependence of the full width at the half maximum (FWHM) of the  $^{75}\text{As}$ -NQR spectrum. To obtain  $H_{\text{int}}(T)$  and  $T_N$ , we employed the following simulation. In a magnetically ordered state, the NQR Hamiltonian is expressed as  $\mathcal{H}_{\text{AFM}} = -^{75}\gamma\hbar\vec{I} \cdot \vec{H}_{\text{int}} + \mathcal{H}_Q$ . As a first step, we assumed  $\vec{H}_{\text{int}} = (0, 0, H_{\text{int}})$ , as was found in the underdoped iron pnictide [30]. As shown schematically in the inset to Fig. 3(a), the energy levels of the nuclear spins change and the  $^{75}\text{As}$ -NQR spectrum splits into two peaks at  $\nu^{\text{AFM}} = \nu_Q \pm ^{75}\gamma H_{\text{int}}$  below  $T_N$ . The NQR spectrum at  $T = 4.2$  K can be reproduced by a sum of the two Lorentzian

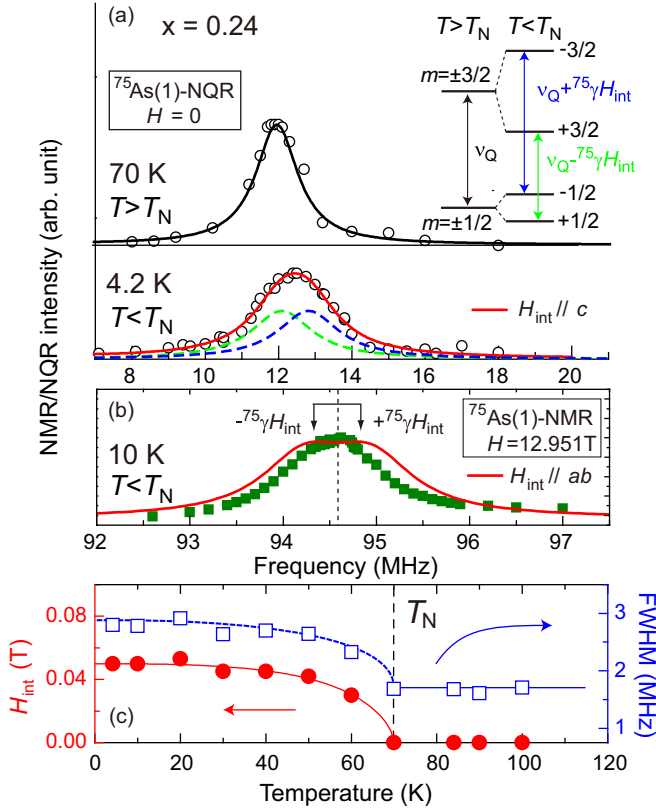


FIG. 3. (Color online) (a) The  $^{75}\text{As}$ -NQR spectrum for As(1) above and below  $T_N$  for  $x = 0.24$ . The dotted and solid curves are the results of fitting (see text). The inset shows a schematic view of the NQR transition levels. (b) The  $^{75}\text{As}$ -NMR spectrum for As(1) below  $T_N$  for  $x = 0.24$ . The dotted line indicates the  $\theta = 90^\circ$  peak position ( $f_\perp$ ). The solid curve is a sum of the two Lorentzian curves centered at  $f_\perp \pm 75\gamma H_{\text{int}}$ . (c) Temperature dependences of the FWHM of the  $^{75}\text{As}$ (1)-NQR spectrum and  $H_{\text{int}}$  for  $x = 0.24$ . The dotted curve and solid horizontal line on FWHM( $T$ ) are guides to the eye. The solid line on  $H_{\text{int}}(T)$  is the mean-field fit. The dashed vertical line indicates  $T_N$ .

curves centered at  $\nu^{\text{AFM}}$ . This indicates that the  $H_{\text{int}}$  below  $T_N$  is spatially uniform. On the other hand, if we assume the  $\vec{H}_{\text{int}}$  is parallel to the  $ab$  plane, it can also reproduce the NQR spectrum with  $H_{\text{int}} = 0.05$  T [28]. However, as seen in Fig. 3(b), the  $\vec{H}_{\text{int}} \parallel ab$  plane, which generates an in-plane internal field of  $\pm H_{\text{int}}$  at the As site, is inconsistent with the NMR spectrum. Rather, it seems consistent with the  $\vec{H}_{\text{int}} \parallel c$  direction, which just shifts the peak position and makes the NMR spectrum width broad [13]. And hence,  $\vec{H}_{\text{int}} = (0, 0, H_{\text{int}})$  below  $T_N$  is the most plausible in this case. The obtained  $H_{\text{int}}(T)$  is plotted in Fig. 3(c). The solid curve is a fit to the mean-field theory that gives a  $T_N = 70$  K. This is exactly the temperature at which  $1/T_1 T$  shows a peak. From these results, we conclude that the peak in  $1/T_1 T$  is due to the onset of an antiferromagnetic order.

As seen in Fig. 2(d), the antiferromagnetic order occurs in the highly electron-doped region ( $x \geq 0.15$ ) in the present system, while the antiferromagnetic phase is completely suppressed in  $\text{LnFeAsO}_{1-x}\text{F}_x$  [2–8] and  $\text{Ba}(\text{Fe}_{1-x}\text{TM}_x)_2\text{As}_2$  [10–12] at a much lower doping concen-

tration. Notably,  $T_N$  increases with increasing doping. The mechanism of the increase of  $T_N$  by doping is unclear at the present stage. One possibility is that the nesting between enlarged Fermi surfaces due to electron doping [31,32] can act to enhance the antiferromagnetism [33].

Next, we discuss the possible magnetic structure below  $T_N$ . According to a previous report [30], the  $\vec{H}_{\text{int}}$  at the As site can be written as the sum of the contribution from the four nearest-neighbor Fe sites as  $\vec{H}_{\text{int}} = \sum_{i=1}^4 \tilde{B}_i \cdot \vec{m}_i$ , where  $\tilde{B}_i$  is the hyperfine coupling tensor consisting of the components  $B_{\alpha\beta}$  ( $\{\alpha, \beta\} = a, b, c$ ) between the As nucleus and  $i$ th Fe site, and  $\vec{m} = (m_a, m_b, m_c)$  is the magnetic moment at the Fe site. First, we compare with the ordering vector  $\vec{q} = (\pi, 0, 0)$  or  $(\pi, 0, \pi)$  found in the underdoped iron pnictides [30]. In this case,  $\vec{m}$  produces  $\vec{H}_{\text{int}} = 4B_{ac}(m_c, 0, m_a)$ . Using  $B_{ac} = 0.43$  T/ $\mu_B$  [30], we obtain  $m_a \sim 0.03\mu_B$ , which yields  $H_{\text{int}} = 0.05$  T. However, this value would be one order of magnitude smaller than that observed in  $\text{LaFeAsO}$  ( $m_{\text{Fe}} = 0.36\mu_B$ ,  $T_N = 137$  K) [34] and  $\text{BaFe}_2\text{As}_2$  ( $m_{\text{Fe}} = 0.87\mu_B$ ,  $T_N = 143$  K) [35]. Below we consider other possibilities. The first one is  $\vec{q} = (\pi, \pi, 0)$  or  $(\pi, \pi, \pi)$ . In this case,  $\vec{H}_{\text{int}}$  is perpendicular to the  $c$  direction [30] and can be ruled out. The second one is  $\vec{q} = (0, \pi, 0)$  or  $(0, \pi, \pi)$ , which produces  $\vec{H}_{\text{int}} = 4B_{bc}(0, m_c, m_b)$ . This type of magnetic structure has recently been discovered in  $\text{LaFeAsO}_{0.49}\text{H}_{0.51}$  with  $m_a = 1.21\mu_B$  and  $T_N = 89$  K [21]. Obviously, this does not produce  $H_{\text{int}}$  at the As site. The observed spatially distributed  $H_{\text{int}}$  [22] may be because this antiferromagnetic state is accompanied by a structural transition, which causes a displacement of As and Fe atoms about  $0.13$  Å in the  $a$  direction [21]. Our system is similar to this situation. The As atom in  $\text{Ca}_{1-x}\text{La}_x\text{FeAs}_2$  also exhibits a small displacement of  $0.03$  Å in the  $a$  direction originating from its monoclinic crystal structure [23]. Therefore, although a further quantitative understanding is difficult, this may explain the present results. In fact, such an order was predicted by the band calculation for  $\text{CaFeAs}_2$  [36]. We call for neutron diffraction measurements to determine the magnetic structure for  $\text{Ca}_{1-x}\text{La}_x\text{FeAs}_2$ .

Figure 4 summarizes the phase diagram of  $\text{Ca}_{1-x}\text{La}_x\text{FeAs}_2$ . We find that antiferromagnetism in  $\text{Ca}_{1-x}\text{La}_x\text{FeAs}_2$  is robust against doping. Furthermore,  $T_N$  increases with increasing doping. This phase diagram is qualitatively similar to the heavily doped  $\text{LaFeAsO}_{1-x}\text{H}_x$  [20,21]. However, there are two fundamental differences between them. First, the heavily doped  $\text{LaFeAsO}_{1-x}\text{H}_x$  shows a structural phase transition above  $T_N$  [21], but it has not been observed in  $\text{Ca}_{1-x}\text{La}_x\text{FeAs}_2$  [23]. Second, the situation regarding the relationship between antiferromagnetism and superconductivity is completely different. In heavily doped  $\text{LaFeAsO}_{1-x}\text{H}_x$ , the antiferromagnetic phase and superconductivity are completely segregated [22], but they coexist microscopically in  $\text{Ca}_{1-x}\text{La}_x\text{FeAs}_2$ , as elaborated below.

Figure 5 shows the temperature dependence of  $1/T_1$  [28]. For all La concentration,  $1/T_1$  decreases rapidly below  $T_N$ , in accordance with the uniform  $H_{\text{int}}(T)$  (see Fig. 3). As shown in the inset to Fig. 5, the bulk nature of superconductivity for  $x = 0.15$  and  $0.19$  is confirmed by the large superconducting shielding fractions and further assured by the distinct reduction of  $1/T_1$  below  $T_c$ . These results indicate that antiferromagnetism and superconductivity coexist microscopically for

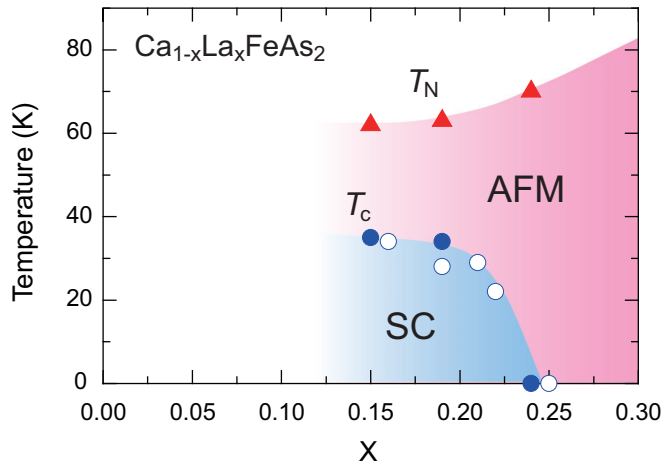


FIG. 4. (Color online) Phase diagram for  $\text{Ca}_{1-x}\text{La}_x\text{FeAs}_2$ . AFM and SC denote the antiferromagnetically ordered metal and superconducting state. Open circles are from the magnetization results for another batch of samples [24].

$x = 0.15$  and  $0.19$ . Furthermore,  $1/T_1$  shows  $1/T_1 T = \text{const}$  behavior well below  $T_N$  for  $x = 0.24$ , suggesting that the heavily doped  $\text{Ca}_{1-x}\text{La}_x\text{FeAs}_2$  is an antiferromagnetic metal. For  $x = 0.15$  and  $0.19$ ,  $1/T_1$  decreases rapidly again below  $T_c(H)$ , as was found previously [14–17]. It is worth noting that  $1/T_1$  at low temperatures in the superconducting state becomes proportional to  $T$ . In the superconducting state coexisting with an antiferromagnetic order, the spin rotation is broken so that a spin-triplet component can be mixed [37]. Our observation may be a reflection of such a phenomenon, since the spin-triplet state will have nodes in the gap function. More work in this regard is needed.

In summary, we have presented systematic NMR/NQR studies on the La-doped iron pnictide  $\text{Ca}_{1-x}\text{La}_x\text{FeAs}_2$ . We find doping-enhanced antiferromagnetism that microscopically coexists with superconductivity. Since the lattice parameters in  $\text{Ca}_{1-x}\text{La}_x\text{FeAs}_2$  do not change by doping, the unusual evolution of antiferromagnetism and superconductivity compared

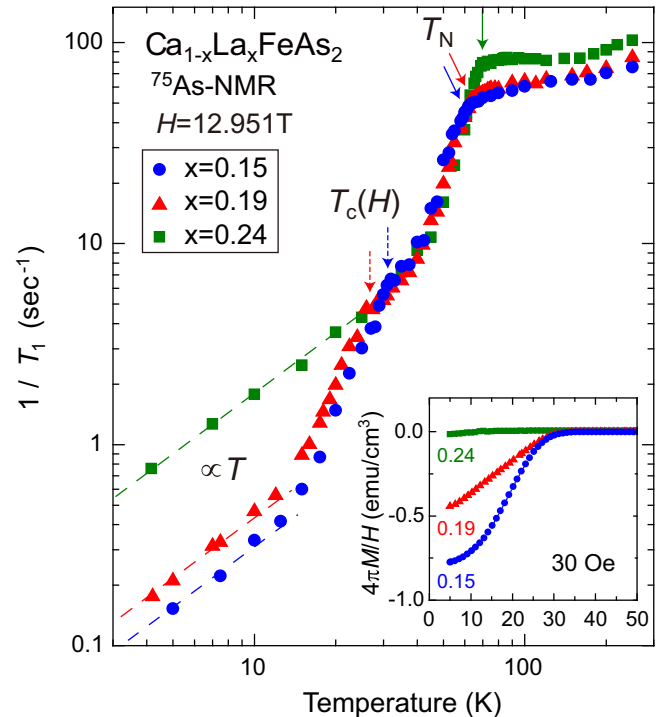


FIG. 5. (Color online) Temperature dependence of  $1/T_1$ . The solid and dotted arrows indicate  $T_N$  and  $T_c(H)$ , respectively. The dashed lines indicate the relation  $1/T_1 T = \text{const}$ . The inset shows the temperature dependences of the magnetization.

with other iron pnictides originates purely from doped carriers. The present results provide further opportunities and different perspectives for understanding the role of doped carriers and the mechanism of high- $T_c$  superconductivity in iron pnictides.

We thank S. Onari for discussions. This work was supported in part by research grants from MEXT (No. 22103004, No. 25400372, No. 25400374, No. 26287082, No. 15H01047, and No. 15H05852).

- [1] P. A. Lee, N. Nagaosa, and X.-G. Wen, Doping a Mott insulator: Physics of high-temperature superconductivity, *Rev. Mod. Phys.* **78**, 17 (2006).
- [2] Y. Kamihara, T. Watanabe, M. Hirano, and H. Hosono, Iron based layered superconductor  $\text{La}[\text{O}_{1-x}\text{F}_x]\text{FeAs}$  ( $x = 0.05\text{--}0.12$ ) with  $T_c = 26$  K, *J. Am. Chem. Soc.* **130**, 3296 (2008).
- [3] Z.-A. Ren, J. Yang, W. Lu, W. Yi, X.-L. Shen, Z.-C. Li, G.-C. Che, X.-L. Dong, L.-L. Sun, F. Zhou, and Z.-X. Zhao, Superconductivity in the iron-based F-doped layered quaternary compound  $\text{Nd}[\text{O}_{1-x}\text{F}_x]\text{FeAs}$ , *Europhys. Lett.* **82**, 57002 (2008).
- [4] Z.-A. Ren, J. Yang, W. Lu, W. Yi, G.-C. Che, X.-L. Dong, L.-L. Sun, and Z.-X. Zhao, Superconductivity at 52 K in iron based F doped layered quaternary compound  $\text{Pr}[\text{O}_{1-x}\text{F}_x]\text{FeAs}$ , *Mater. Res. Innovations* **12**, 105 (2008).
- [5] C. Wang, L. Li, S. Chi, Z. Zhu, Z. Ren, Y. Li, Y. Wang, X. Lin, Y. Luo, S. Jiang, X. Xu, G. Cao and Z. Xu, Thorium-doping-induced superconductivity up to 56 K in  $\text{Gd}_{1-x}\text{Th}_x\text{FeAsO}$ , *Europhys. Lett.* **83**, 67006 (2008).
- [6] Z.-A. Ren, W. Lu, J. Yang, W. Yi, X.-L. Shen, Z.-C. Li, G.-C. Che, X.-L. Dong, L.-L. Sun, F. Zhou, and Z.-X. Zhao, Superconductivity at 55 K in iron-based F-doped layered quaternary compound  $\text{Sm}[\text{O}_{1-x}\text{F}_x]\text{FeAs}$ , *Chin. Phys. Lett.* **25**, 2215 (2008).
- [7] G. F. Chen, Z. Li, D. Wu, G. Li, W. Z. Hu, J. Dong, P. Zheng, J. L. Luo, and N. L. Wang, Superconductivity at 41 K and Its Competition with Spin-Density-Wave Instability in Layered  $\text{CeO}_{1-x}\text{F}_x\text{FeAs}$ , *Phys. Rev. Lett.* **100**, 247002 (2008).
- [8] J.-W. G. Bos, G. B. S. Penny, J. A. Rodgers, D. A. Sokolov, A. D. Huxley, and J. P. Attfield, High pressure synthesis of late rare earth  $R\text{FeAs}(\text{O},\text{F})$  superconductors;  $R = \text{Tb}$  and  $\text{Dy}$ , *Chem. Commun.* **31**, 3634 (2008).
- [9] M. Rotter, M. Pangerl, M. Tegel, and D. Johrendt, Superconductivity and crystal structures of  $(\text{Ba}_{1-x}\text{K}_x)\text{Fe}_2\text{As}_2$  ( $x = 0\text{--}1$ ), *Angew. Chem., Int. Ed.* **47**, 7949 (2008).
- [10] X. F. Wang, T. Wu, G. Wu, R. H. Liu, H. Chen, Y. L. Xie, and X. H. Chen, The peculiar physical properties and phase diagram

- of  $\text{BaFe}_{2-x}\text{Co}_x\text{As}_2$  single crystals, *New J. Phys.* **11**, 045003 (2009).
- [11] L. J. Li, Y. K. Luo, Q. B. Wang, H. Chen, Z. Ren, Q. Tao, Y. K. Li, X. Lin, M. He, Z. W. Zhu, G. H. Cao, and Z. A. Xu, Superconductivity induced by Ni doping in  $\text{BaFe}_2\text{As}_2$  single crystals, *New J. Phys.* **11**, 025008 (2009).
- [12] P. C. Canfield, S. L. Bud'ko, Ni Ni, J. Q. Yan, and A. Kracher, Decoupling of the superconducting and magnetic/structural phase transitions in electron-doped  $\text{BaFe}_2\text{As}_2$ , *Phys. Rev. B* **80**, 060501(R) (2009).
- [13] Z. Li, R. Zhou, Y. Liu, D. L. Sun, J. Yang, C. T. Lin, and G.-q. Zheng, Microscopic coexistence of antiferromagnetic order and superconductivity in  $\text{Ba}_{0.77}\text{K}_{0.23}\text{Fe}_2\text{As}_2$ , *Phys. Rev. B* **86**, 180501(R) (2012).
- [14] R. Zhou, Z. Li, J. Yang, D. L. Sun, C. T. Lin, and G.-Q. Zheng, Quantum criticality in electron-doped  $\text{BaFe}_{2-x}\text{Ni}_x\text{As}_2$ , *Nat. Commun.* **4**, 2265 (2013).
- [15] F. L. Ning, K. Ahilan, T. Imai, A. S. Sefat, M. A. McGuire, B. C. Sales, D. Mandrus, P. Cheng, B. Shen, and H.-H. Wen, Contrasting Spin Dynamics Between Underdoped and Overdoped  $\text{Ba}(\text{Fe}_{1-x}\text{Co}_x)_2\text{As}_2$ , *Phys. Rev. Lett.* **104**, 037001 (2010).
- [16] T. Oka, Z. Li, S. Kawasaki, G. F. Chen, N. L. Wang, and G.-Q. Zheng, Antiferromagnetic Spin Fluctuations Above the Dome Shaped and Full-Gap Superconducting States of  $\text{LaFeAsO}_{1-x}\text{F}_x$  Revealed by  $^{75}\text{As}$ -Nuclear Quadrupole Resonance, *Phys. Rev. Lett.* **108**, 047001 (2012).
- [17] M. Hirano, Y. Yamada, T. Saito, R. Nagashima, T. Konishi, T. Toriyama, Y. Ohta, H. Fukazawa, Y. Kohori, Y. Furukawa, K. Kihou, C. Lee, A. Iyo, and H. Eisaki, Potential antiferromagnetic fluctuations in hole-doped iron-pnictide superconductor  $\text{Ba}_{1-x}\text{K}_x\text{Fe}_2\text{As}_2$  studied by  $^{75}\text{As}$  nuclear magnetic, *J. Phys. Soc. Jpn.* **81**, 054704 (2012).
- [18] S. Iimura, S. Matsuishi, H. Sato, T. Hanna, Y. Muraba, S. W. Kim, J. E. Kim, M. Takata, and H. Hosono, Two-dome structure in electron-doped iron arsenide superconductors, *Nat. Commun.* **3**, 943 (2012).
- [19] J. Yang, R. Zhou, L. L. Wei, H. X. Yang, J. Q. Li, Z. X. Zhao, and G.-Q. Zheng, New superconductivity dome in  $\text{LaFeAsO}_{1-x}\text{F}_x$  accompanied by structural transition, *Chin. Phys. Lett.* **32**, 107401 (2015).
- [20] N. Fujiwara, S. Tsutsumi, S. Iimura, S. Matsuishi, H. Hosono, Y. Yamakawa, and H. Kontani, Detection of Antiferromagnetic Ordering in Heavily Doped  $\text{LaFeAsO}_{1-x}\text{H}_x$  Pnictide Superconductors Using Nuclear-Magnetic-Resonance Techniques, *Phys. Rev. Lett.* **111**, 097002 (2013).
- [21] M. Hiraishi, S. Iimura, K. M. Kojima, J. Yamaura, H. Hiraka, K. Ikeda, P. Miao, Y. Ishikawa, S. Torii, M. Miyazaki, I. Yamauchi, A. Koda, K. Ishii, M. Yoshida, J. Mizuki, R. Kadono, R. Kumai, T. Kamiyama, T. Otomo, Y. Murakami, S. Matsuishi, and H. Hosono, Bipartite magnetic parent phases in the iron oxypnictide superconductor, *Nat. Phys.* **10**, 300 (2014).
- [22] R. Sakurai, N. Fujiwara, N. Kawaguchi, Y. Yamakawa, H. Kontani, S. Iimura, S. Matsuishi, and H. Hosono, Quantum critical behavior in heavily doped  $\text{LaFeAsO}_{1-x}\text{H}_x$  pnictide superconductors analyzed using nuclear magnetic resonance, *Phys. Rev. B* **91**, 064509 (2015).
- [23] N. Katayama, K. Kudo, S. Onari, T. Mizukami, K. Sugawara, Y. Sugiyama, Y. Kitahama, K. Iba, K. Fujimura, N. Nishimoto, M. Nohara, and H. Sawa, Superconductivity in  $\text{Ca}_{1-x}\text{La}_x\text{FeAs}_2$ : A novel 112-type iron pnictide with arsenic zigzag bonds, *J. Phys. Soc. Jpn.* **82**, 123702 (2013).
- [24] K. Kudo, T. Mizukami, Y. Kitahama, D. Mitsuoka, K. Iba, K. Fujimura, N. Nishimoto, Y. Hiraoka, and M. Nohara, Enhanced superconductivity up to 43 K by P/Sb doping of  $\text{Ca}_{1-x}\text{La}_x\text{FeAs}_2$ , *J. Phys. Soc. Jpn.* **83**, 025001 (2014).
- [25] K. Kudo, Y. Kitahama, K. Fujimura, T. Mizukami, H. Ota, and M. Nohara, Superconducting transition temperatures of up to 47 K from simultaneous rare-earth element and antimony doping of 112-type  $\text{CaFeAs}_2$ , *J. Phys. Soc. Jpn.* **83**, 093705 (2014).
- [26] H. Yakita, H. Ogino, T. Okada, A. Yamamoto, K. Kishio, T. Tohei, Y. Ikuhara, Y. Gotoh, H. Fujihisa, K. Kataoka, H. Eisaki, and J. Shimoyama, A new layered iron arsenide superconductor:  $(\text{Ca},\text{Pr})\text{FeAs}_2$ , *J. Am. Chem. Soc.* **136**, 846 (2014).
- [27] NMR/NQR measurements were carried out by using a phase-coherent spectrometer and at a fixed magnetic field of  $H = 12.951$  T. Typical pulse sequence  $10 \mu\text{s} - \tau - 20 \mu\text{s}$  with  $\tau = 25 \mu\text{s}$  is used to obtain spin echo.
- [28] See Supplemental Material at <http://link.aps.org/supplemental/10.1103/PhysRevB.92.180508> for the recovery curves to obtain  $T_1$  and the result of simulation with  $\vec{H}_{\text{int}} \parallel ab$  plane.
- [29] A. Abragam, *The Principles of Nuclear Magnetism* (Oxford University Press, London, 1961).
- [30] K. Kitagawa, N. Katayama, K. Ohgushi, M. Yoshida, and M. Takigawa, Commensurate itinerant antiferromagnetism in  $\text{BaFe}_2\text{As}_2$ :  $^{75}\text{As}$ -NMR studies on a self-flux grown single crystal, *J. Phys. Soc. Jpn.* **77**, 114709 (2008).
- [31] X. Liu, D. Liu, L. Zhao, Q. Guo, Q. Mu, D. Chen, B. Shen, H. Yi, J. Huang, J. He, Y. Peng, Y. Liu, S. He, G. Liu, X. Dong, J. Zhang, C. Chen, Z. Xu, Z. Ren, and X. J. Zhou, Fermi surface and band structure of  $(\text{Ca},\text{La})\text{FeAs}_2$  superconductor from angle-resolved photoemission spectroscopy, *Chin. Phys. Lett.* **30**, 127402 (2013).
- [32] M. Y. Li, Z. T. Liu, W. Zhou, H. F. Yang, D. W. Shen, W. Li, J. Jiang, X. H. Niu, B. P. Xie, Y. Sun, C. C. Fan, Q. Yao, J. S. Liu, Z. X. Shi, and X. M. Xie, Significant contribution of As  $4p$  orbitals to the low-lying electronic structure of the 112-type iron-based superconductor  $\text{Ca}_{0.9}\text{La}_{0.1}\text{FeAs}_2$ , *Phys. Rev. B* **91**, 045112 (2015).
- [33] S. Onari, Y. Yamakawa, and H. Kontani, High- $T_c$  Superconductivity Near the Anion Height Instability in Fe-Based Superconductors: Analysis of  $\text{LaFeAsO}_{1-x}\text{H}_x$ , *Phys. Rev. Lett.* **112**, 187001 (2014).
- [34] C. de la Cruz, Q. Huang, J. W. Lynn, J. Li, W. Ratcliff II, J. L. Zarestky, H. A. Mook, G. F. Chen, J. L. Luo, N. L. Wang, and P. Dai, Magnetic order close to superconductivity in the iron-based layered  $\text{LaO}_{1-x}\text{F}_x\text{FeAs}$  systems, *Nature (London)* **453**, 899 (2008).
- [35] Q. Huang, Y. Qiu, W. Bao, M. A. Green, J. W. Lynn, Y. C. Gasparovic, T. Wu, G. Wu, and X. H. Chen, Neutron-Diffraction Measurements of Magnetic Order and a Structural Transition in the Parent  $\text{BaFe}_2\text{As}_2$  Compound of FeAs-Based High-Temperature Superconductors, *Phys. Rev. Lett.* **101**, 257003 (2008).
- [36] X. Wu, C. Le, Y. Liang, S. Qin, H. Fan, and J. Hu, Effect of As-chain layers in  $\text{CaFeAs}_2$ , *Phys. Rev. B* **89**, 205102 (2014).
- [37] A. Hinojosa, R. M. Fernandes, and A. V. Chubukov, Time-Reversal Symmetry Breaking Superconductivity in the Coexistence Phase with Magnetism in Fe Pnictides, *Phys. Rev. Lett.* **113**, 167001 (2014).